UCRL--100211

DE90 011467

MODELING OF ZIRCALOY CLADDING DEGRADATION UNDER REPOSITORY CONDITIONS

Lakshman Santanam, Suresh Raghavan, Henry Shaw* and Bryan A. Chin

Department of Materials Engineering, Auburn University, Alabama

* Lawrence Livermore National Laboratory, Livermore, California

*This work was performed under the auspices of the U.S. Department of Energy by Lawrence Livermore National Laboratory under contract No. W-7405-Eng-48.

Modeling of Zircaloy Cladding Degradation Under Repository Conditions

Lakshman Santanam
Graduate Research Assistant
Materials Engineering
Auburn University
Auburn, Alabama 36849

Suresh Raghavan
Graduate Research Assistant
Materials Engineering
Auburn University
Auburn, Alabama 36849

Henry Shaw
Technical Area Leader
Release Rates, NWMP
Lawrence Livermore National Laboratory
P.O. Box 808, L-204
Livermore, California 94550

Bryan A. Chin
Professor and Chairman
Materials Engineering
Ross Hall
Auburn University
Auburn, Alabama 36849

Abstract

Two potential degradation mechanisms, creep and stress corrosion cracking, of Zircaloy cladding during repository storage of spent nuclear fuel have been investigated. The deformation and fracture map methodology has been used to predict maximum allowable initial storage temperatures to achieve a thousand year life without rupture as a function of spent-fuel history. A stress analysis of fuel rods has been performed. Stresses in the outer zirconium oxide layer and the inner Zircaloy tube have been predicted for typical internal pressurization, oxide layer thickness, volume expansion from formation of the oxide layer and thermal expansion coefficients of the cladding and oxide. Stress relaxation occurring in-reactor has also been taken into account. The calculations indicate that for the anticipated storage conditions investigated, the outer zirconium oxide layer is in a state of compression thus making it unlikely that stress corrosion cracking of the exterior surface will occur.

Key Terms: Zircaloy, repository, creep, stress corrosion, deformation and fracture maps, stress analysis, stress relaxation

Introduction

Repository storage is one of the long-term solutions to the disposal of spent nuclear fuel that is being investigated. The Department of Energy's Office of Civilian Radioactive Waste Management has recently chosen to concentrate investigations into the suitability of tuffaceous rocks at the Yucca mountain Nevada test site for high-level radioactive waste disposal. Regulatory requirements specify that the engineered barrier must not release more than one part in 10^5 of the 1000 year inventory of radionuclides each year for a period of 10,000 years.[1,2] The Zircaloy cladding that already exists on the fuel rod may be an important barrier that contributes to the ability to meet the above release requirement. This paper presents results from an investigation conducted in support of studies designed to address the integrity of the Zircaloy cladding during storage in a tuff repository.

Three distinct time periods can be identified during repository storage:[3]

1. The high-temperature period during which the container is assumed to be unbreached, the fuel rods are surrounded by inert gas or air and no liquid water is present.
2. The intermediate-temperature period when the container is assumed to be unbreached and liquid water (from breached fuel rods containing water) may be present and in contact with the fuel rods.
3. The lower-temperature period when the container is assumed to be breached and air, water vapor and liquid water may be in contact with the spent fuel rods. J-13 well water comes closest to the aqueous environment that will invade the breached canister.[4] The composition of J-13 well water may be found in reference 2.

Several potential mechanisms of Zircaloy cladding degradation during dry storage have been identified such as hydride reorientation, stress corrosion cracking, creep and creep fraccure. A summary discussion of potential mechanisms of degradation is given by reference 2. This paper addresses only two of the mechanisms of spent fuel rod degradation, creep/creep fracture and exterior surface stress corrosion cracking.

Creep and long-term fracture damage occurs during the inert gas isolation phase of the storage (period one). Deformation and fracture map analyses have been used to predict the time to rupture of Zircaloy clad spent Light Water Reactor (LWR) fuel subjected to various storage conditions. The questions that this analysis attempts to answer are how long and under what temperature conditions the fuel can be stored and reasonably claimed to be unfailed. During repository storage, temperatures are anticipated to rise first as the repository is filled and then decrease with increasing time due to a decay in the heat generation rate of the spent fuel. In this analysis, a life fraction rule has been used to account for changing temperature and stress conditions. This life fraction rule has been combined with the results of deformation and fracture maps to predict maximum allowable storage temperatures to achieve a 1000 year life.

Stress corrosion cracking of the exterior surface of the spent fuel rod is the second failure mode that has been analyzed. An aqueous environment could initiate stress corrosion cracking on the outside of an unbreached rod during periods two and three. A stress analysis of fuel rods was carried out. The model was constructed using a thick cylindrical shell of Zircaloy with an outer thin shell of zirconium oxide. A change in the internal radius of the oxide was calculated that results from the volume expansion of the oxide upon formation, temperature changes during cooling of the repository, and a compressive force on the oxide due to the difference in lattice parameters between monoclinic oxide and the Zircaloy cladding. A change in the external radius of the cladding was calculated that results from a tensile force in the cladding due to volume expansion of the oxide, temperature change effects, and internal pressure. Equating these changes in radii resulted in an equation for the only unknown parameter, the stress in the oxide layer, which was found to be compressive. The magnitude of the compressive stress in the oxide layer after accounting for stress relaxation that occurs in the Zircaloy cladding

in - reactor was estimated to be 800 MPa (120 Ksi). Densities of Zircaloy and zirconium oxide were measured and a multiplication factor was used to approximate deviations of these values due to irradiation and directionally dependent volume expansion. A computer program was developed to predict stresses in the oxide and the cladding as a function of the above parameters.

Objectives

The objectives of this work were:

1. To determine the maximum allowable peak temperatures at which spent fuel can be stored and reasonably be claimed to be unfailed for a period of 1000 years;

2. To model the stress state in the spent fuel cladding and determine if stress corrosion cracking was a probable mechanism of degradation for the stress state determined.

Deformation and Fracture Maps

Background

One of the probable mechanisms of failure during the inert gas isolation phase of the storage is creep rupture failure. Previous predictions of Zircaloy cladding failure have been based on direct extrapolation of existing short term data [5,6] or have assumed a single equation, like the Larson Miller parameter [7], to describe the failure mechanisms. These methods ignore changes in the deformation and failure mechanisms as the stress and temperature conditions are altered and resulting failure times change. Such analyses are very useful for interpolation between existing data fields but oftentimes lead to erroneous results when extrapolated to regimes involving different deformation and failure phenomenon.

Deformation and fracture maps enable predictions of the dominant deformation and failure mode for varying temperature and stress regimes, as well as varying irradiation histories.[8] Deformation and fracture maps can be generated using the model based method in which different theoretical expressions for deformation or fracture are evaluated. The mechanism with the highest deformation rate is assumed to be the dominate mechanism. Similarly, in the generation of a model based fracture map, values of time to failure are numerically evaluated for possible fracture mechanisms, with the assumption that the mechanism with the shortest failure time controls the fracture. An empirical life fraction rule is combined with the results of the deformation and fracture maps to predict acceptable storage temperatures.

Analysis Method

The deformation and fracture map methodology has been applied in the licensing of several dry storage facilities. A detailed description of the methodology can be found in reference 8. The present work describes modifications to dry

storage deformation and fracture maps to predict 1000 year cladding response for assumed repository storage conditions. This included the selection of a function to model the anticipated temperature decay history of the repository, refinement of the parameters that control the recovery process to better describe the region of lower repository temperatures, and incorporation of variable time steps to improve the accuracy of cumulative damage predictions at short times when the temperature is changing rapidly.

Selection of temperature decay function. The projected peak cladding temperature as a function of time for storage in a Tuff repository is shown in Figure 1[2]. This temperature history is based upon horizontal emplacement in a repository at 44 kW/acre of a canister containing 10 year old spent fuel (3.3 kW) with 12 internal fins. This temperature curve can be approximated by the equation given below, which was then incorporated into the models:

$$T\ (K) = T_o\ (K) * (\text{time in months})^{-0.1041} \qquad (1)$$

Selection of melting temperature. The experimental melting temperature of beta phase Zircaloy, used in the dry storage predictions, was replaced by the theoretical melting temperature of alpha phase Zircaloy (calculated to be 1900 K). Based upon a review of the pertinent literature [9] regarding the use of the theoretical melting temperature of alpha zirconium, it was concluded that a better description of the annealing and dislocation motion process (which occur in the alpha Zircaloy phase), could be obtained by using the theoretical alpha Zircaloy melting temperature instead of the beta Zircaloy melting temperature. All applications of the deformation and fracture map models to repository storage involve only the alpha phase. Use of the beta Zircaloy melting temperature results in a prediction that underestimates the recovery process.[9]

Incorporation of variable time steps. Another modification involved incorporation of variable time steps to calculate the cumulative damage. Small time steps correspond to small temperature and stress changes, which improve the accuracy of cumulative damage calculations. The variable time step employed utilizes small time steps when the temperature is changing rapidly and larger steps as the rate of temperature change decreases.

Calculations

Table 1 lists the deformation equations used in the analyses and Table 2 lists the coefficients and the symbols used in the equations. Table 3 lists the reduced deformation equations after substitution of these coefficients. Table 4 lists the fracture equations; Table 5 shows the symbols and coefficients used in these equations and Table 6 lists the reduced fracture equations.

Deformation rates were evaluated from the equations listed in Table 3. The dominant deformation mechanism is the one with the highest deformation rate. Values of time to failure were determined from the equations in Table 6. The mechanism with the least time to failure controls the fracture. Note that the equations in Table 6 are dependent upon the deformation rate which is

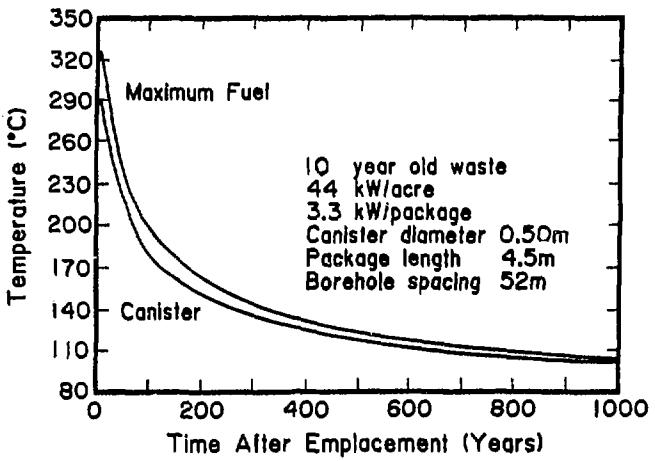

FIGURE 1. PEAK FUEL AND CONTAINER TEMPERATURE AS A FUNCTION OF TIME (AFTER ROTHMAN REFERENCE 2)

Table 1

Deformation Equations

High Temperature Climb	$\dot{\epsilon}_{HT} = A_1 \cdot D_{ol} \cdot \exp(-Q_1/RT) \cdot \frac{Eb}{KT} \cdot (\sigma/E)^n$
Low Temperature Climb	$\dot{\epsilon}_{LT} = 50 \cdot A_1 \cdot D_{oc} \cdot \exp(-Qc/RT) \cdot \frac{Eb}{KT} \cdot (\sigma/E)^{n+2}$
Grain Boundary Sliding	$\dot{\epsilon}_{GBS} = A_{GBS} \cdot D_{ogb} \cdot \exp(-Qgb/RT) \cdot \frac{Eb}{KT} \cdot (b/d)^3 \cdot (\sigma/E)^2$
Nabarro-Herring	$\dot{\epsilon}_{NH} = A_{NH} \cdot D_{ol} \cdot \exp(-Q_1/RT) \cdot \frac{Eb}{KT} \cdot (b/d)^2 \cdot (\sigma/E)^2$
Coble	$\dot{\epsilon}_{CO} = A_{CO} \cdot D_{ogb} \cdot \exp(-Qgb/RT) \cdot \frac{Eb}{KT} \cdot (b/d)^3 \cdot (\sigma/E)$

Table 2

Symbols and Coefficient Values for Deformation Equations

$\dot{\epsilon}$ = strain rate

σ = stress

T = temperature

R = gas constant = 8.3144 J/mole-K

k = Boltzmann's constant = 1.38×10^{-29} MJ/K

b = Burger's vector = 3.23×10^{-10} m

d = grain size = 5.0×10^{-6} m

T_m = melting temperature of Zircaloy = 1900K

E = Young's Modulus $(11.81 - 13.0434577\ T/T_m) \times 10^4$ MPa for $T_m/T > 3.63$
$(11.09 - 10.3793382\ T/T_m) \times 10^4$ MPa for $T_m/T < 3.63$

n = stress exponent = 5

Q = activation energy

Q_l = 250 kJ/mol

Q_{gb} = 175 kJ/mol

Q_c = 180 kJ/mol

D_o = diffusivity coefficient

D_{ol} = 2.00×10^{-4} m^2/s

D_{ogb} = 3.89×10^{-6} m^2/s

D_{oc} = 2.26×10^{-6} m^2/s

A = strain rate coefficient

A_l = 7.4×10^3

A_{CO} = 5.34×10^8

A_{GBS} = 8.81×10^{12}

A_{NH} = 9.2×10^5

A_{GBL} = 5×10^2

Table 3

Reduced Deformation Equations

High Temperature Climb	$\ln\dot{\varepsilon}_{HT} = 5\cdot\ln(\sigma/E) + 55.86204969 - 15.82774316(T_m/T) + \ln(T_m/T) + \ln(E/10^4)$
Low Temperature Climb	$\ln\dot{\varepsilon}_{LT} = 7\cdot\ln(\sigma/E) + 55.29204967 - 11.39821221(T_m/T) + \ln(T_m/T) + \ln(E/10^4)$
Grain Boundary Sliding	$\ln\dot{\varepsilon}_{GBS} = 2.1\ln(\sigma/E) + 20.85204971 - 11.07785422(T_m/T) + \ln(T_m/T) + \ln(E/10^4)$
Nabarro-Herring	$\ln\dot{\varepsilon}_{NH} = \ln(\sigma/E) + 18.36204972 - 15.82774317\ (T_m/T) + \ln(T_m/T) + \ln(E/10^4)$
Coble	$\ln\dot{\varepsilon}_{CO} = \ln(\sigma/E) + 11.14205004 - 11.07785429(T_m/T) + \ln(T_m/T) + \ln(E/10^4)$

Table 4

Fracture Equations

Theoretical Shear Strength	$\sigma_{th} = \left(\frac{E\gamma_f}{a_o}\right)^{1/2} \approx \frac{E}{10}$
Transgranular Fracture	$t_f^{TG} = \epsilon_n + \left(\frac{1}{4.937}\right)\left(\frac{n}{n-1}\right)\ln\frac{0.38}{f_v^{1/2}} \cdot 1\ \dot{\epsilon}^{-1}$
Triple-Point Cracking	$t_f^{TP} = \frac{f}{Ed}\left(\frac{\sigma}{E}\right)^{-1}\dot{\epsilon}^{-1}$
Cavitation-Diffusional Growth	$t_f^{CD} = \frac{2.525 \times 10^{-3}\ \ell^3}{\delta D_{ogb} b^2 \exp\frac{-Q_{gb}}{RT}}\left(\frac{kT}{Eb}\right)\left(\frac{\sigma}{E}\right)^{-1}$
Cavitation--Power Law Growth	$t_f^{CP} = \frac{(1 - 0.78\ P_o\ \ell_o)}{4.87}\dot{\epsilon}^{-1}$

Table 5

Symbols and Coefficient Values for Fracture Equations

t_f = time to fracture

ϵ_n = hole nucleation strain = 0.08

f_v = volume fraction of intragranular inclusions = 0.025

P_o = average particle diameter = 100 Å

ℓ_o = particle spacing along boundary = 2.0×10^{-6} m

ζ = $\dot{\epsilon}_{GBS}/\dot{\epsilon}$ = contribution of grain boundary strain rate to total strain rate = 0.2

ℓ = average cavity spacing = 2.6×10^{-6} m (6 per grain segment)

δ = width of grain boundary = 1.6×10^{-8} m (50 Burger's vectors)

γ_f = free surface energy created by fracture = 35 J/m^2

a_o = lattice spacing

Table 6

Reduced Fracture Equations

Transgranular Fracture	$\ln t_f^{TG} = -1.797 - \ln\dot{\epsilon}$
Triple-Point Cracking	$\ln t_f^{TP} = -5.655 - \ln\dot{\epsilon} - \ln\frac{\sigma}{E} - \ln\frac{E}{10^4}$
Cavitation--Diffusional Growth	$\ln t_f^{CD} = +4.15 - \ln\dot{\epsilon}_{gbs} + \ln\frac{\sigma}{E}$
Cavitation--Power Law Growth	$\ln t_f^{CP} = -1.587 - \ln\dot{\epsilon}$

calculated from the Equations of Table 3. A detailed description of the development of the equations and their use is given in reference 8.

A life fraction rule was used to account for changing temperature and stress conditions. Temperatures are assumed to decrease with increasing time as per equation (1) after the initial warm up period. Additionally the stress in the cladding will decrease due to cladding creep and a decrease in the fission gas pressure due to decreasing temperature. Small increases due to helium gas production from actinide decay were neglected for this 1000 year analysis. This life fraction rule can be mathematically represented as follows:

$$1 = \frac{\Delta t_1}{\tau_1} + \frac{\Delta t_2}{\tau_2} + \frac{\Delta t_3}{\tau_3} + \ldots, \qquad (2)$$

or

$$\sum_{i=1}^{N} \frac{\Delta t_i}{\tau_i} = 1 \qquad (3)$$

where Δt_i is the time spent at the i^{th} temperature, and τ_i is the time required to fracture a specimen under isothermal, isostress testing conditions. When the cumulative damage fraction ($\Delta t_i/\tau_i$) reaches one, the fuel rod is assumed to have failed.

Results

It is assumed that the fuel rods will have a temperature decay history as described by equation 1. To determine the maximum allowable storage temperatures, a computer program was developed. This program uses the deformation and fracture map methodology in conjunction with the life fraction rule to predict behavior during repository storage. The results are depicted in Figure 2, which is a plot of Maximum Allowable Peak Storage Temperature as a function of clad hoop stress for 10 year old spent fuel (10 years in wet storage) and an initial clad stress of 70 MPa. This maximum Allowable Temperature is the maximum peak storage temperature (for a given initial clad stress) following the temperature decay rate shown in Figure 1 that yields a cumulative damage fraction of less than one after an elapsed time of 1000 years. For times of 1000 years and beyond the damage accumulation rates are so low (because of the low repository temperatures) that calculations beyond 1000 years is not necessary.

For typically stressed rods (70 -100 MPa) with low fission gas release, initial storage temperatures of 340°C would be acceptable. However for high burnup rods with large fission gas release that results in highly stressed rods (140-160 MPa), initial storage temperatures should not exceed 300°C. It should be noted that the predicted maximum allowable temperature is a function of initial clad stress (fuel rod history), age of spent fuel (cumulative time spent in wet storage) and anticipated temperature history of the repository. The calculations are conservative for spent fuel that is younger than 10 years of age, but nonconservative for fuel rods that are greater than 10 years of

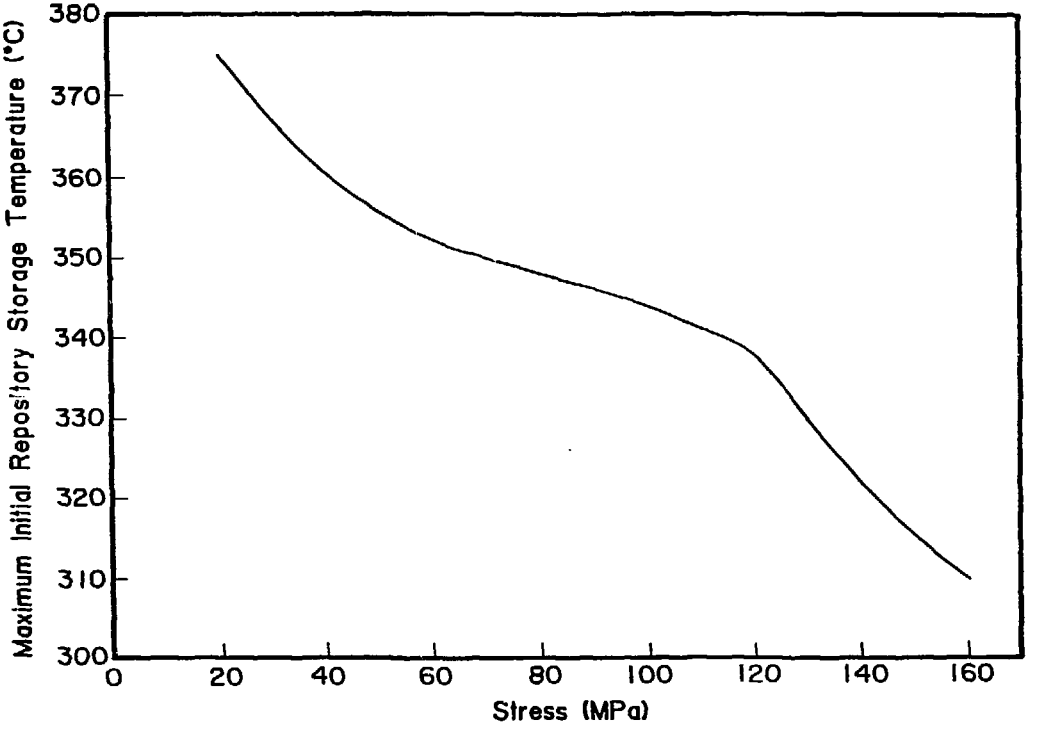

FIGURE 2. PREDICTED MAXIMUM INITIAL REPOSITORY STORAGE TEMPERATURE FROM A 1000 YEAR DEFORMATION AND FRACTURE MAP ANALYSIS.

age. This dependence upon spent fuel age results from the higher rates of temperature decay in younger spent fuel versus older spent fuel. Additionally, the temperature history curve shown in Figure 1 does not include the initial region of temperature increase that occurs during filling of the repository.

Stress Analysis of Fuel Rods

Background

As already mentioned, stress corrosion cracking of the exterior cladding surface is a possibility during periods two and three of repository storage. The fuel rod is comprised of an outer thin layer of zirconium oxide on an inner substrate of Zircaloy. The zirconium oxide acts as a passive film protecting the substrate from attack by chemicals, which in conjunction with the internal stresses in the fuel rod can cause stress corrosion cracking. To ensure that the Zircaloy is not exposed to stress corrosion cracking attack by some chemicals, it is necessary that cracks do not develop in the oxide layer, or preexisting cracks (formed during fabrication or handling) do not grow through the oxide layer. A compressive stress in the oxide layer will ensure this requirement. The aim of this work has been to predict the stress state in the oxide under assumed storage conditions and identify regimes where there is a tensile stress in the oxide.

The stress state in the cladding and the oxide layer are dependant on the following parameters:

1. The internal pressure on the cladding arising from prepressurization of the fuel rods with additional pressure resulting from fission gas release.
2. The volume expansion of the oxide layer. Because the densities of zirconium oxide and Zircaloy are different, the oxide layer undergoes a volume change on formation.
3. Different thermal expansion coefficients of Zircaloy and the oxide give rise to stresses on cooling.
4. The assumption that the oxide adheres perfectly to the substrate also gives rise to additional stresses.

The volume expansion was calculated from lattice parameter measurements on unirradiated Zircaloy specimens. The results are listed in the section below and the modeling effort has been described in the section following the experimental results.

Experimental Results

Density measurements were carried out on Zircaloy and zirconium oxide to estimate the volume expansion of the oxide. Lattice parameter measurements were performed on powder samples of the materials at room temperature and densities were calculated from these values. Table 7 lists the measured lattice parameters, estimates of the densities based on these measurements and values obtained from literature. It can be seen that the measured values are in excellent agreement with those obtained from other sources.

Table 7

Lattice Parameters and Densities of Zircaloy and Zirconium Oxide

Material	Lattice Parameters and Structure (Measured)	Density (Calculated)	Density (Literature)	Reference
Zircaloy	a = 3.23 Å c = 5.13 Å Hexagonal Close Packed	6.54 gm/cm^3	6.5 gm/cm^3	10
Zirconium oxide	a = 5.10 Å b = 5.12 Å c = 5.31 Å β = 99.30° Monoclinic	5.71 gm/cm^3	5.4 to 6.02 gm/cm^3	11

From the measured density values of Zircaloy (6.54 gm/cm^3) and zirconium oxide (5.71 gm/cm^3), an estimate of the volume expansion coefficient (v), was made as follows:

$$v = \frac{\text{Volume of oxide - Volume of Zircaloy}}{\text{Volume of Zircaloy}} \quad (4)$$

This calculation yielded an expansion value of 0.54. Upper and lower bounds were set on this value using the range of density values of zirconium oxide obtained from literature. The calculation yielded a minimum expansion coefficient value of 0.4 and a maximum value of 0.68.

Stress Distributions

The model was developed under the following assumptions:

1. The oxide layer adheres perfectly to the substrate.
2. The strains in the oxide layer along the radial direction, the tangential direction and the lengthwise direction are the same and each equals one third the volume expansion.
3. Poisson's ratio equals one third.
4. The stress in the oxide layer is elastic and the stress in the Zircaloy is elastic/plastic.

Irradiation effects and directionally dependent volume expansion were taken into account by assigning maximum and minimum bounds to volume expansion values. Figure 3 is a schematic of the cross section of a fuel rod. The dimensions shown are typical values and were obtained from reference 4. Table 8 lists the parameters used in the model along with numerical values. The source of the values is also indicated.

The change in the internal radius of the oxide has three terms; the first due to volume expansion, the second due to the imposed condition that the oxide adhere perfectly to the substrate and the third due to the thermal contraction effects, and is given by the following expression:

$$\Delta R(\text{oxide}) = vr_2/3 - Fr_2^2/t_2E_2 - \alpha_2 r_2 \Delta T \quad (5)$$

The stress - strain relationship assumed for the Zircaloy is given by:[18]

$$\sigma = K\epsilon^n \quad (6)$$

The values of the material constant, K, and the strain hardening exponent, n, were estimated using tensile test data on irradiated Zircaloy from Yaggee et. al.[16]

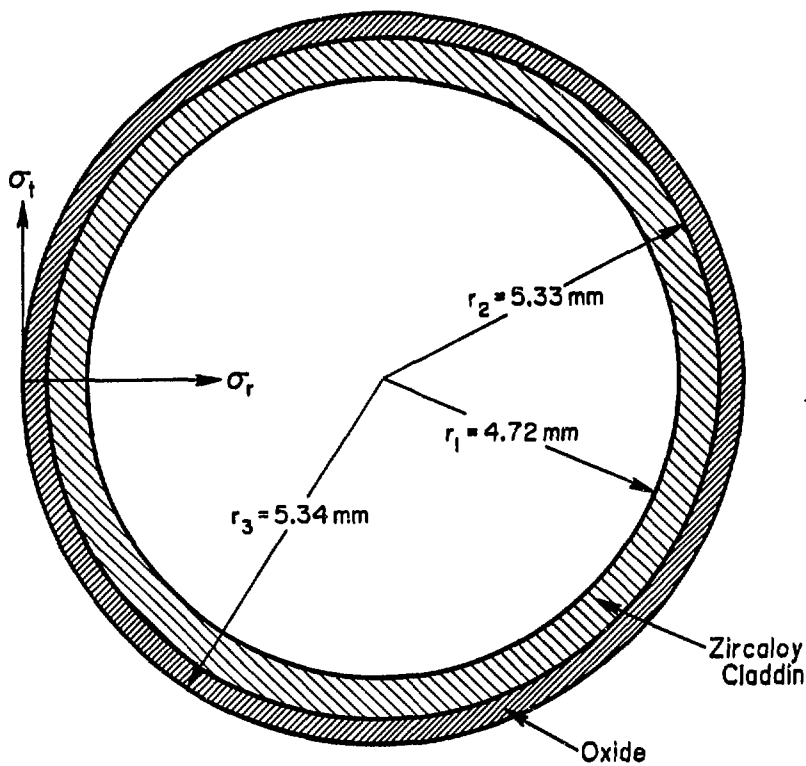

FIGURE 3. SCHEMATIC OF THE CROSS SECTION OF A FUEL ROD.

Table 8

Parameters in the Model to Predict Stress Distributions

Parameter	Description	Value	Reference
r_1	inner radius of the cladding	$4.72 * 10^{-3}$ m (0.186 inches)	4
r_2	radial distance to oxide	$5.33 * 10^{-3}$ m (0.21 inches)	4
t_1	thickness of the cladding	$6.09 * 10^{-4}$ m (0.024 inches)	4
t_2	thickness of the oxide	10 μm ($3.94 * 10^{-4}$ inches)	4
E_1	Modulus of Zircaloy	79594 MPa ($11.5 * 10^6$ psi)	2
E_2	Modulus of zirconium oxide	210328 MPa ($30.5 * 10^6$ psi)	13
v	volume expansion value	0.42 (minimum) - 0.68 (maximum) 0.54 (measured)	
P	internal pressure on cladding	0 - 21 MPa (range assumed)	
μ	Poisson's ratio	1/3 (assumed)	
α_1	thermal expansion coefficient of Zircaloy	$8.37 * 10^{-6}$/°C	14
α_2	thermal expansion coefficient of zirconium oxide	$7.2 * 10^{-6}$/°C	15
ΔT	temperature decrease during repository storage	250 K (typical value chosen)	
K	material constant for Zircaloy	395448 MPa	17
n	strain hardening exponent	0.34	17
r	radial position on cladding where stress is to be determined		
F	force of adherence between oxide and cladding		
σ_o	hoop stress in oxide		
σ_r	radial stress in cladding		
σ_t	tangential stress in cladding		

The change in external radius of the cladding is similarly given by[17]:

$$\Delta R(\text{cladding}) = \frac{r_2(\sigma_t - \mu\sigma_r)^{1/n}}{K^{1/n}} - \alpha_t r_2 \Delta T \qquad (7)$$

where the expressions for the radial and tangential stresses (Table 9) have to be evaluated at r_2.

Equating (5) and (7) results in an equation for F, the force in the oxide layer. The final expressions for F are shown in Table 9. The first equation for force comes from an elastic deformation only analysis where both the oxide and Zircaloy were assumed to obey Hook's Law. The second equation for force comes from inclusion of plastic deformation following the above sequence of equations (5-7).

Table 9 lists the final equations for evaluating the hoop stress in the oxide, and the radial and tangential stresses in the cladding once the force is known.

Results

Using the equations developed, calculations were completed for an internal pressure range from 0 to 21 MPa (0 to 3000 psi; typical value 1300 psi or 8.96 MPa), and volume expansion values from a minimum of 0.4 to a maximum of 0.68 (measured value 0.54). Tangential and radial stresses in the cladding and hoop stresses in the oxide were evaluated. A temperature decrease of 250°C was assumed in these calculations, which is greater than that assumed over the repository storage life.

Figure 4 is a plot of the tangential stress in the cladding and the hoop stress in the oxide as a function of radial position for an internal pressure of 8.96 MPa (1300 psi) for three volume expansion values - 0.4, 0.54 and 0.68. The yield stress of irradiated Zircaloy (700 MPa) is shown by a straight line. It can be seen that as the volume expansion value increases, the magnitude of the stresses also increases. The tangential stress in the cladding is a maximum at the internal radius and varies linearly as a function of the radial position. The difference in magnitude of the tangential stresses at the inside radius and the Zircaloy-oxide boundary is about 10%. The hoop stresses in the oxide are compressive in nature with a large magnitude. It should be noted here that the stress in the oxide layer is a constant throughout the thickness. The reason for this being that the oxide film thickness was modeled as a thin cylinder.

Similar calculations were completed for internal pressures of 0 and 21 MPa. The stress distributions were similar; the magnitude of the tangential stresses are higher for the 21 MPa case than the 8.96 MPa case by about 5-10%; the hoop stress in the oxide is reduced by a very small factor (0.7%). For the 0 MPa case, the tangential stresses in the cladding are lower by about 10% than the 8.96 MPa case. The hoop stresses in the oxide layer are slightly higher (0.4%).

σ_t tangential stress in cladding

Table 9

Final Equations to Determine Stresses

Equation for force in oxide layer (Elastic Analysis)

$$F = \frac{vr_2/3 - \dfrac{2Pr_1^2r_2}{E_1(r_2^2-r_1^2)} + r_2\Delta T(\alpha_1-\alpha_2)}{\dfrac{r_2(r_1^2+r_2^2)}{E_1(r_2^2-r_1^2)} + \dfrac{r_2^2}{t_2E_2} - \dfrac{\mu r_2}{E_1}}$$

Equation for force in oxide layer (Plastic Analysis)

$$F^{1/n}\left\{\frac{(r_1^2+r_2^2)^{1/n}}{[K(r_2^2-r_1^2)]^{1/n}} - \frac{\mu^{1/n}}{K^{1/n}}\right\} + \frac{Fr_2}{t_2E_2} = v/3 + \Delta T(\alpha_1-\alpha_2) - \left\{\frac{(2Pr_1^2)^{1/n}}{[K(r_2^2-r_1^2)]^{1/n}}\right\}$$

Equations to compute stresses

$$\sigma_o = -Fr_2/t_2$$

$$\sigma_t = \frac{Pr_1^2 + Fr_2^2 + (r_1^2r_2^2/r^2)(P+F)}{r_2^2 - r_1^2}$$

$$\sigma_r = \frac{-Fr_2^2 - Pr_1^2 + (r_1^2r_2^2/r^2)(P+F)}{r_2^2 - r_1^2}$$

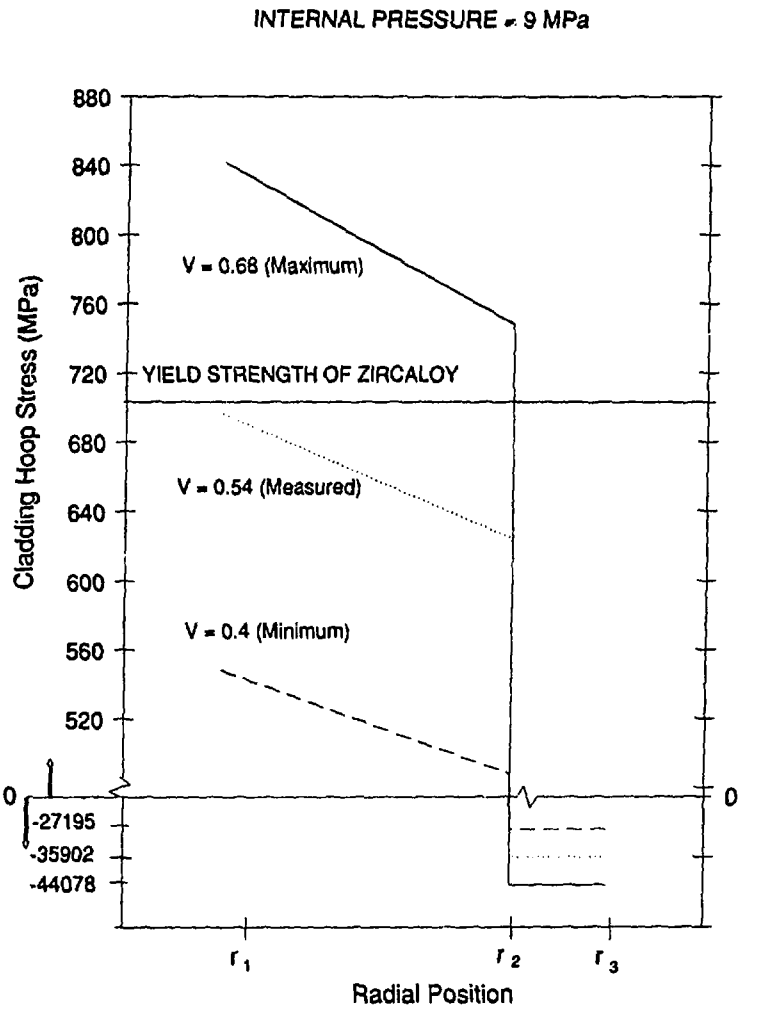

FIGURE 4. PREDICTED HOOP STRESS AS A FUNCTION OF RADIAL POSITION.

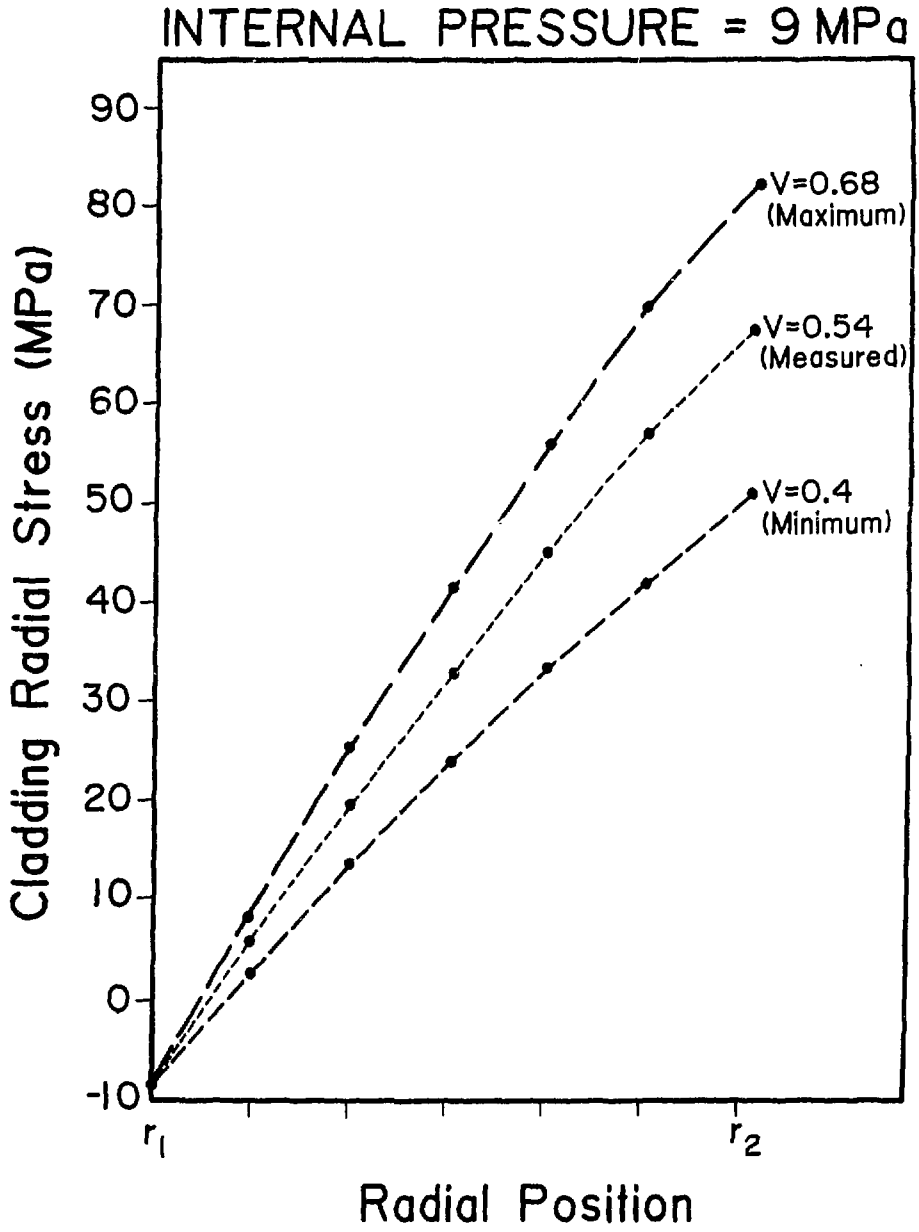

FIGURE 5. PREDICTED RADIAL STRESS AS A FUNCTION OF RADIAL POSITION.

Figure 5 is a plot of the radial stress in the Zircaloy as a function of radial position for an internal pressure of 8.96 MPa for three expansion coefficients - 0.4, 0.54 and 0.68. The stress distribution is approximately linear with the inside of the cladding in a state of compression and the clad-oxide boundary in a state of tension; the magnitude of the stress at the inside surface is the same for all three expansion coefficients - 8.96 MPa (1300 psi). The stress gradient across the thickness of the cladding increases as the expansion coefficient increases. The radial stresses are lower by a factor of 10 than the tangential stresses. As anticipated, the tangential stresses dominate.

Calculations of radial stresses were performed for internal pressure values of 0 MPa and 21 MPa. The magnitude of the radial stress at the internal radius of the cladding varies as a function of internal pressurization and is the same for all expansion coefficients; it is 0 for the 0 MPa case and 21 for the 21 MPa case. But there is hardly any difference in the magnitude of the stress at the clad-oxide boundary for a given oxide volume expansion value. That is to say, assuming an expansion value of 0.4, the radial stresses are within 1% of each other for all internal pressure values. The same holds true for all other expansion values.

Discussion

The magnitude of the stresses predicted by these analyses are higher than the yield stress of Zircaloy. However, in the absence of detailed experimental data, such an analysis enables predictions as to the nature of the stress state in the oxide layer and the cladding. Stress relaxation occurring in - reactor is a factor that lowers the stresses in the cladding. This effect lowers the stress in the oxide layer also. This is described in the following section.

Stress Relaxation

After oxide formation, the Zircaloy cladding during normal operation in - reactor undergoes irradiation enhanced creep. This leads to stress relaxation in the cladding. To maintain its adherence to the cladding and its continuous nature, the stresses in the oxide layer are also lowered correspondingly. The final stress distribution in the cladding after accounting for stress relaxation was determined and a force balance on the Zircaloy-zirconium oxide composite ring was performed to estimate the magnitudes of the stresses in the cladding and the oxide layer.

The creep rate was calculated using the deformation and fracture map models presented in the beginning of this paper. The creep rate equation describing deformation for this temperature region can be approximated in the form (Table 1):

$$\dot{\varepsilon}_p = K_1 \sigma^n \qquad (8)$$

The value assumed for the constant K_1 is $5.24 * 10^{-26}$ $1/MPa^n$-sec

The equation for the elastic tangential strain can be determined from:

$$\epsilon_e = \sigma_t/E_1 \tag{9}$$

Knowing the initial stress distribution in the cladding, the final stress distribution after stress relaxation can be determined from the following equation:[18]

$$1/\sigma_f^{\,n+1} = 1/\sigma_i^{\,n+1} + K_1 E_1 (n+1)t \tag{10}$$

where n is the stress exponent (equals 5) and t is the time in seconds (nominally four years).

A force balance then yields:

$$2\sigma_o t_2 - 2Pr_1 = -2\int \sigma_t dr \tag{11}$$

The term $\int \sigma_t dr$ is the area under the curve of a tangential stress in the cladding versus radial position plot. Using a computer routine, the relaxed tangential stresses in the cladding were evaluated as a function of radial position. Simpson's rule[19] was used to calculate the $\sigma_t dr$ term. The only unknown in the equation is the hoop stress in the oxide which was then determined.

Results and Discussion

Figure 6 is a plot of tangential stress in the cladding and hoop stress in the oxide layer as a function of radial position for three volume expansion coefficients - 0.4, 0.54 and 0.68. All these calculations were performed for an internal pressure of 8.96 MPa (1300 psi) in the cladding, which is a typical value for spent fuel. It can be seen that the final stresses in the cladding after stress relaxation are lowered by a factor of 7. The stress distribution is linear in the cladding. The corresponding stress in the oxide layer is lowered to about 800 MPa (120 Ksi) compression. This stress is, again, constant as a function of oxide thickness as the oxide is being modeled as a thin cylinder. It can also be seen that the final stresses in the cladding and the oxide are nearly the same for different values of expansion coefficients.

A literature search was performed to determine the ultimate strength in compression of zirconium oxide. A reasonable value for this quantity is in the order of 2400 MPa (350 Ksi).[20] The final stresses in the cladding and the oxide layer are, hence in the elastic region. The oxide layer is thus in a state of compression, even after creep of the cladding has been taken into account.

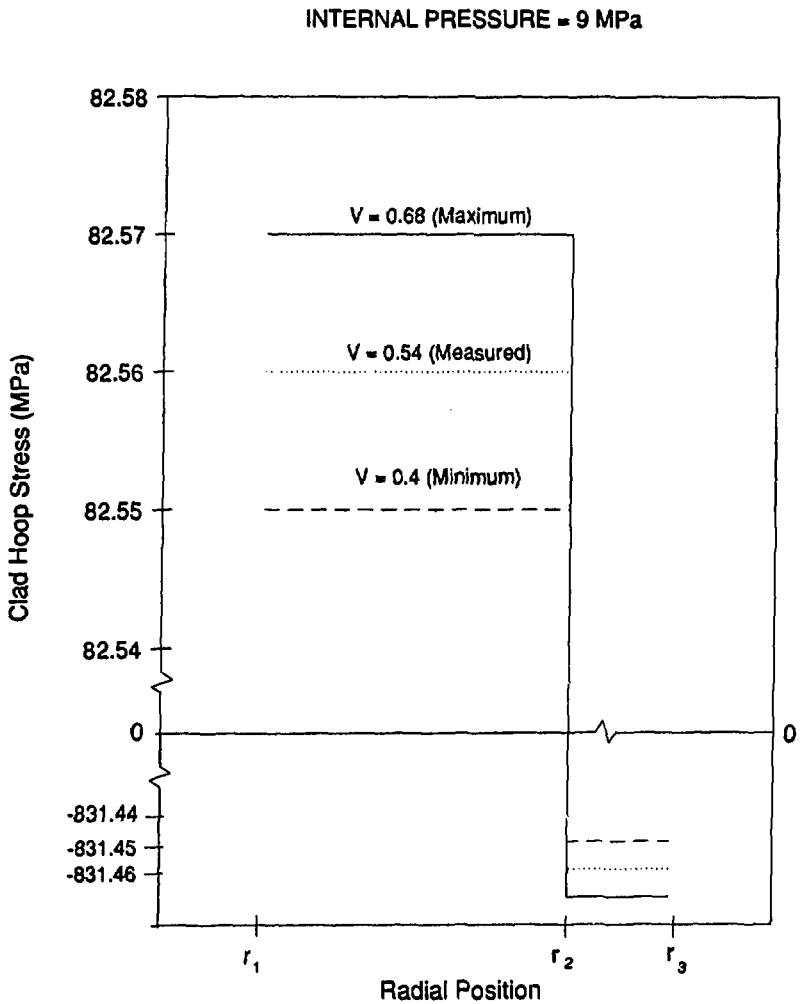

FIGURE 6. PREDICTED RELAXED HOOP STRESS AS A FUNCTION OF RADIAL POSITION.

The analysis above has only dealt with the center region of the spent fuel rod which sees the highest temperature due to the fuel column and therefore is the most likely to fail either by creep or stress corrosion cracking attack. Admittedly hemispherical or angular geometry at the end caps will require a different stress analysis. However stress corrosion cracking is sensitive to temperature and would be anticipated to occur in the peak temperature region.

Conclusions

Zircaloy cladding is potentially an effective barrier to the release of radionuclides from spent fuel stored in a repository. After making some assumptions about Zircaloy material behavior and oxide film formation on the Zircaloy, preliminary models have been developed to address maximum storage temperature limits and exterior surface stress corrosion cracking of the Zircaloy cladding. The following conclusions resulted from this preliminary study:

1. Based on a deformation and fracture map analysis, predictions of maximum allowable storage temperatures for cladding stresses from 20 MPa to 160 MPa have been made for repository storage up to 1000 years. Maximum allowable temperatures are 340°C (613 K) for typically stressed rods (70 -100 MPa) and 300°C (573 K) for highly stressed rods (140 -160 MPa).

2. Using a preliminary conceptual model for stress and displacement response of Zircaloy cladding surrounded by a thin film of oxide, a large compressive hoop stress in the outer oxide layer of spent fuel cladding was calculated. This makes it highly unlikely that classical stress corrosion cracking of the exterior cladding surface can occur under these conditions.

Sponsorship

This work was performed for the Yucca Mountain Project (YMP) under the direction of the University of California, Lawrence Livermore National Laboratory as part of the U.S. Department of Energy Office of Civilian Radioactive Waste Management Program. The Yucca Mountain Project work is managed by the Yucca Mountain Project Office (YMPO) of the U.S. Department of Energy, Nevada Operations Office (DOE/NV).

Acknowledgements

The authors are indebted to Dr. Ray Stout, Lawrence Livermore National Laboratory, California, and Dr. Nels Madsen, Auburn University, for the many useful discussions.

References

1. U. S. Office of the Federal Register Code of Federal Regulations, Title 10, Energy, Part 60, Subpart D, Section 60.113, "Disposal of High-Level Radioactive Wastes in Geologic Repositories: Licensing Procedures."

2. A. J. Rothman, "Potential Corrosion and Degradation Mechanisms of Zircaloy Cladding on Spent Nuclear Fuel in a Tuff Repository," UCID-20172, September 1984.

3. H. D. Smith, "Zircaloy Cladding Corrosion Degradation in a Tuff Repository," HEDL-7455, Rev.1, July 1985, p. 12.

4. H. D. Smith, "Initial report on Stress Corrosion Cracking Experiments Using Zircaloy-4 Spent Fuel Cladding Rings," Westinghouse Hanford Company, Richland, WA.

5. L. D. Blackburn et. al., "Maximum Allowable Temperature for Storage of Spent Nuclear Fuel - An Interim Report," HEDL-TME 78-37, UC-70, 1978.

6. E. R. Einziger, D. M. Bozi, and A. K. Miller, "Transactions," Waste Form Development and Processing, American Nuclear Society, 1980, p.131.

7. A. K. Miller, "Application of the SCCIG Model to Dry Storage of Spent Fuel," Workshop on Spent Fuel Integrity in Dry Storage, Seattle, WA, Jan. 20, 1982.

8. M. A. Khan, N. H. Madsen, and B. A. Chin, "Fracture Predictions in Zircaloy Fuel Cladding," Effects of Radiation on Materials: Twelfth International Symposium, ASTM Stp 870, Philadelphia, 1985, pp. 642-655.

9. A. J. Ardell, "On the Calculation of Melting Temperatures for Low-Temperature phases of Polymorphic Metals," Acta Metallurgica, Vol. 11, June 1963, pp. 591-594.

10. W. B. Pearson, Handbook of Lattice Spacings and Structures of Metals and Alloys, Vol. 1, p. 130.

11. JCPDS Card Number 13-307, Structure of zirconium oxide.

12. H. Stehle, F. Garzarolli, A. M. Garde, P. G. Smerde, Zirconium in the Nuclear Industry: Sixth International Symposium, ASTM STP 824, 1984, pp. 483-506.

13. C. F. Smith, and W. B. Crandall, Journal of the American Ceramic Society, Vol. 47, No. 12, December 1964, pp. 624-627.

14. B. Lustman, and F. Kerze, Jr., Editors, The Metallurgy of Zirconium, McGraw Hill Book Company, First Edition, 1955, p. 354.

15. B. G. Parfenov, V. V. Gerasimov, and G. I. Venddiktova, Corrosion of

Zirconium and Zirconium Alloys (Translated from the Russian), Israel Program for Scientific Translations, Jerusalem, 1969, p. 87.

16. F. L. Yaggee, R. F. Mattas, and L. A. Neimark, "Characterization of Irradiated Zircaloys: Susceptibility to Stress Corrosion Cracking", NP-1557, Research Project 1027, prepared by Argonne National Laboratory for EPRI, October 1980, pp. 4-27, Fig. 4-7.

17. F. B. Seely and J. O. Smith, Advanced Mechanics of Materials, Second Edition, John Wiley and Sons, Inc., 1955, pp. 296-299 and p. 305.

18. G. E. Dieter, Mechanical Metallurgy, Second Edition, McGraw Hill Publishing Company, 1976.

19. Erwin Kreyszig, Advanced Engineering Mathematics, Fifth Edition, Wiley Eastern, 1983, p. 789.

20. I-Wei Chen, "Implications of Transformation Plasticity in ZrO_2-Containing Ceramics: II, Elastic-Plastic Indentation," J. Am. Ceram. Soc., 69[3], 1986, p. 192.